SORO-2019-0013-ver9-Sonar_1P
Type: research-article

SOFT ROBOTICS
Volume 00, Number 00, 2019
© Mary Ann Liebert, Inc.
DOI: 10.1089/soro.2019.0013

SoRo
Soft Robotics

ORIGINAL ARTICLE

Closed-Loop Haptic Feedback Control Using a Self-Sensing Soft Pneumatic Actuator Skin

AU1 ▶ Harshal A. Sonar,[1] Aaron P. Gerratt,[2] Stéphanie P. Lacour,[2] and Jamie Paik[1]

Abstract

In this article, we achieve a closed-loop control over haptic feedback, first time for an entirely soft platform. We prototyped a novel self-sensing soft pneumatic actuator (SPA) with soft strain sensors, called SPA-skin, which withstands large multiaxial strains and is capable of high-frequency sensing and actuation. To close-loop control the haptic feedback, the platform requires a cohesively integrated system. Our system consists of a stretchable low profile (<500 μm) SPA and an ultra-compliant thin-metal film strain sensor that create a novel bidirectional platform for tactile sensing via force-tunable vibratory feedback. With this prototype, we demonstrated control of the actuator shape in real time up to 100 Hz at output forces up to 1 N, maintained under variable mechanical loadings. We further characterized the SPA-skin platform for its static and dynamic behavior over a range of actuation amplitudes and frequencies as well as developed an analytical model of this system to predict the actuator inflation state only using the embedded sensor's resistance. Our SPA-skin is a multifunctional multilayer system that can readily be implemented as a high-speed wearable bidirectional interface for contact sensing and vibrotactile feedback.

Keywords: wearable technology, tactile feedback device, liquid metal sensor, strain sensor, soft pneumatic actuators, haptic device

Objective

AU4 ▶ AU3 ▶ Human haptic perception, in addition to visual and auditory feedback, plays a key role in understanding and exploring our local environment.[1] Desktop-scale haptic devices specifically dedicated for providing tactile stimulation have proven their efficacy in various applications, including medical rehabilitation,[2] medical technologies,[3] entertainment, and virtual or augmented reality.[4] More compact vibratory haptic actuators have been integrated into system for human machine interactions, such as car steering wheels and joysticks[5,6]; however, these implementations provide limited physical feedback such as in mobile phones and joysticks that can only modulate its frequency. Furthermore, this frequency modulation is not feedback controlled.

For wearable technology to have accurate physical feedback to the wearer, feedback-controlled actuation is needed. As such, the requirements for wearable devices, which include adaptability and conformability to the body of a human wearer, extend to the haptic technology itself. Existing haptic technologies, however, do not meet the physical requirements necessary to achieve these characteristics. Conformable interfaces interacting with human skin should be made of thin elastic materials that have moduli similar to skin, 0.3–2 MPa.[7–11] This way, the interface can conform to the body and still operate over a wide frequency range (1–400 Hz) and forces up to 1 N.[12] Available tactile feedback devices primarily rely on rigid piezoelectric elements or electromechanical eccentric mass motors.[4,6] Compliant actuators can be developed with elastomeric materials such as soft silicones that have elastic moduli similar to human skin.[7,8,11] The softness and compliance of the soft robotic systems have been useful in many wearable applications ranging from assistive technologies, medical rehabilitation to entertainment.[13–18] Vibrotactile displays using electroactive polymer-based soft actuators have tackled many of the challenges associated with conventional, rigid vibrotactile devices but provide limited wearability as they require high voltages.[12,13]

AU2 ▶ [1]Reconfigurable Robotics Laboratory, Ecole Polytechnique Fédérale de Lausanne, Lausanne, Switzerland.
[2]Laboratory for Soft Bioelectronic Interfaces, School of Engineering, Center for Neuroprosthetics, Ecole Polytechnique Fédérale de Lausanne, Lausanne, Switzerland.

SORO-2019-0013-ver9-Sonar_1P.3d 08/19/19 9:02pm Page 2

Soft material-based pneumatic actuators, composed of elastically inflatable fluidic chambers, have demonstrated their benefits in robotic applications through large-scale deformation and high compliance and have potential to be adapted for wearable haptic applications.[21–28] The major shortcomings for the pneumatic powered actuators are the size of the power supply and the tube length limiting the bandwidth for high frequency of actuation, which need to be separately addressed.

Wearable haptic devices need to ensure that the force imparted on the wearer is consistent with respect to the perceived performance: this depends on how the interface fits and moves with the body. The effective tactile feedback also requires accurate and coherent force transfer from the actuator to the wearer regardless of the external loading or manufacturing variations. This requires embedded sensing of the actuator state and corresponding corrective measures through closed-loop control. There has been significant development in entirely soft and stretchable physical sensors to measure crucial parameters, such as strain and pressure experienced.[13,16,29–32] Advanced manufacturing technologies such as soft three-dimensional (3D) printing have combined soft sensing within soft actuation.[33] Such an integration of soft sensing with soft actuation creates possibility of closed-loop control, which is essential to adapt to the external loading conditions suitable for wearable scenarios. However, no wearable haptic device has demonstrated closed-loop control capabilities with embedded sensing. It has been particularly difficult to design soft stretchable sensors, which can perform under high strains and high strain rates needed for state estimation of high-speed vibratory actuation.

We feedback controlled, for the first time, an entirely soft haptic platform. We experimented this on a novel platform composed of a soft sensor-integrated soft pneumatic actuator (SPA): SPA-skin. Its entirely soft design enables flexible, conformal, and distributable interface over a variety of surfaces. In addition, the integrated sensing and active closed-loop control provide accurate modulation of actuation amplitude and frequency for rich feedback, independent of an external loading.

The major contributions of this work include:

1. Active closed-loop control of soft haptic platform independent of the loading conditions. The closed-loop control compensates for the external disturbance when occurred; therefore, the produced haptic feedback is consistent and accurate.
2. Design of a novel haptic platform that is entirely soft, based on a pneumatic actuation and integrated stretchable liquid metal sensors.
3. Characterization of the SPA-skin for high-fidelity (0–100 Hz) operation and analytical model to estimate the actuator inflation state using sensor resistance.

Materials and Methods

SPA-skin design and manufacturing

The SPA-skin interface, a sensor and actuator laminate, is specifically designed to provide a consistent vibrotactile feedback under variation of the input parameters: amplitude, vibratory frequency, and external loading force (Fig. 1). ◀F1 Amplitude and frequency are the inputs set by the user-need, whereas external loading is dictated by the environmental interactions and disturbance. The sensor-integrated SPA compensates for these three inputs through an active closed-loop feedback control. Here, a seamlessly integrated stretchable strain sensor measures the strain experienced upon the actuator inflation by the resistance change. In case of external loading, the strain value measured is maintained to the set point by actively controlling the input pressure. We also developed a custom data acquisition platform to enable strain sensing and actuation control at high speed (1 kHz) to reliably cover the SPA actuation frequency from 0 to 100 Hz.

The SPA-skin—a sensor and actuator laminate—is composed of soft silicone elastomers and thin biphasic metal films, as depicted in Figure 2a. The actuator layer, SPA, ◀F2 consists of an elastomeric membrane that can be pneumatically inflated with a positive pressure input.[34] This actuator is fabricated with three thin layers: a middle flexible mask layer (50 μm) to define the actuator's shape, sandwiched between

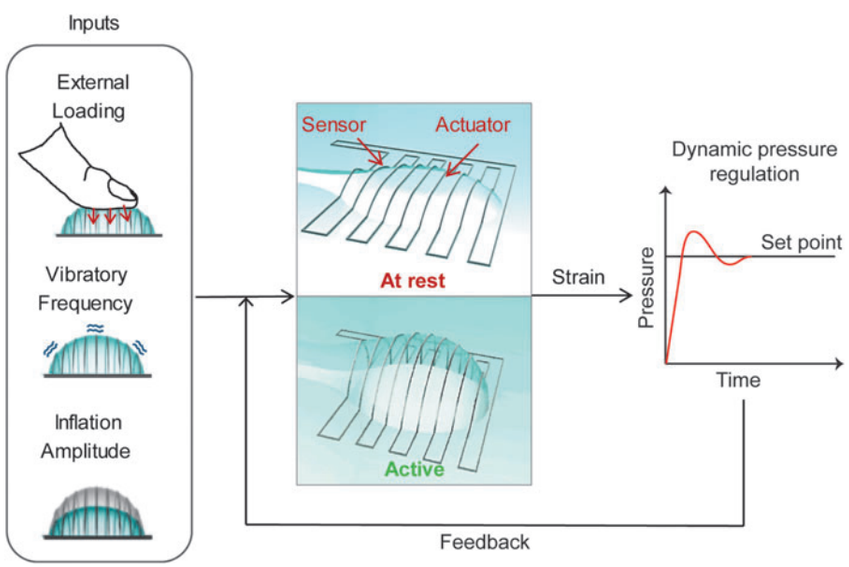


FIG. 1. Overview of the SPA-skin with stretchable resistive strain sensors. The SPA-skin provides a highly conformal interface. A strain sensor of stretchable metallization can be used as the input 4C ▶ to a feedback loop used to control the actuator inflation and exerted force. High-speed data acquisition allows strain sensing and actuation over a range of actuation frequencies from 0 to 100 Hz. SPA, soft pneumatic actuator.

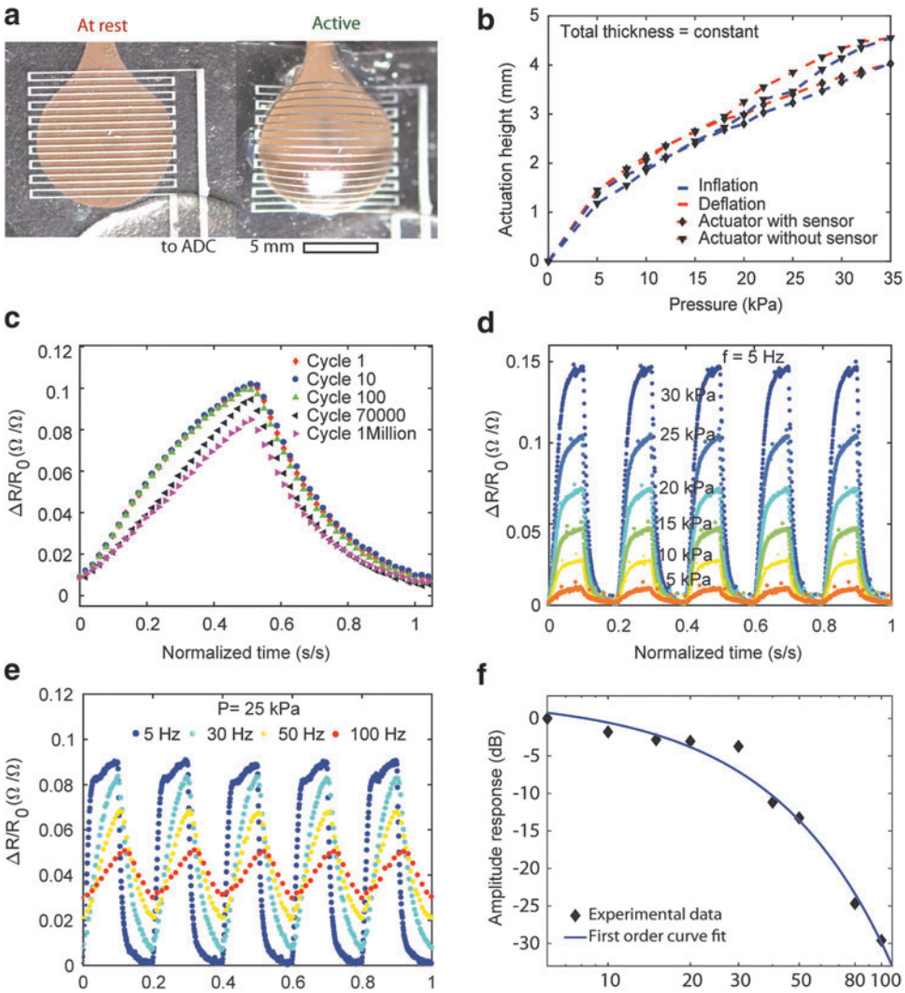


FIG. 2. Characterization of the SPA-skin. **(a)** An SPA-skin prototype before and during inflation. **(b)** Actuators of the same thickness with and without laminated sensors show little change in performance. **(c)** Sensor performance over a million cycles. **(d)** The SPA-skin response for variation input pressure set points from 5 to 30 kPa at 5 Hz. **(e)** The SPA-skin response for variation of actuation frequency from 5 to 100 Hz at 25 kPa pressure set point. **(f)** The SPA-skin amplitude response for variation in actuation frequency. ◀4C

two silicone layers, with a total thickness of 500 μm.[34] The masking layer is laser cut to obtain the desired shape and is then laminated onto the bottom silicone layer to be encapsulated by a thin top silicone layer. The polypropylene mask adheres to the bottom silicone and ensures that, upon inflation, deformation occurs in the top membrane. The actuator geometry is governed by the spatial resolution requirement of 20 mm and force requirement of up to 1 N for sensitivity on the application areas on human back or wrist.[35,36] The actuator area is 10 mm in diameter and has a 2 mm inlet tube. The sensor layer, an eGaIn-filled microchannel membrane, is prepared with a biphasic (liquid–solid) Gallium-based metallization patterned on a thin silicone membrane.[30] It is then laminated on top of the actuator to complete the soft actuator–sensor interface. The layout of the strain sensor covers the entire area of the SPA to record changes in strain upon inflation with positive input pressure. The soft sensor-skin hosts metallic meanders on a 40 μm thick (substrate and encapsulation) on Polydimethylsiloxane (PDMS) film patterned at the resolution limit of the biphasic metallization technique to maximize the sensor sensitivity. The entire SPA-skin is fabricated using PDMS (Dow Corning Sylgard 184) because of its low viscoelasticity[37] and because multiple layers can be covalently bonded with oxygen plasma treatment. The intentional use of the same material for both the actuator and the sensor substrate yields a robust monolithic functional skin with embedded sensing and actuation capabilities. The softness of the SPA-skin manufactured matches with that of the human skin to have a compliant and wearable prototype.

SPA-skin characterization

The frequency range of somatic perception for human skin varies from 0 to 100 Hz for rapidly adapting sensor receptors and 100–400 Hz Pacinian corpuscles.[12] To apply a controlled feedback of the integrated SPA-skin system over such a variety of modulable amplitude and frequency ranges, an accurate model of the steady state and transient behavior is first needed. We therefore perform static and dynamic characterization of the SPA-skin to obtain all relevant system parameters necessary for implementing closed-loop control.

Static characterization. Despite the addition of extra sensor layer, we observed a minimal mechanical loading on the SPA with less than 10% change in the actuator inflation (Fig. 2b). The covalent bonding between sensor and actuator layers ensures the conformity of the sensor layer around the SPA during inflation. This enables the accurate measure of the strain experienced by the SPA through the soft sensors,

SORO-2019-0013-ver9-Sonar_1P.3d 08/19/19 9:02pm Page 4

even at high strain rates. Upon inflation of the SPA, the resistance of the soft sensor increases due to the increase in biaxial strain. The gauge factor (GF) observed for the stretchable metallization is approximately unity and independent of the strain rate (Supplementary Movie S1). The SPA-skin system exhibited a robust behavior, with less than 10% deviation in the relative change in resistance ($\Delta R/R$) obtained during high strain rate operation at 20 Hz to a pressure of 25 kPa for a million cycles (Fig. 2c). Such a robustness highlights the ability of the SPA-skin to be used in the wearable applications over long duration under dynamic operation. The sensors also demonstrate rapid response times under 1 ms, meeting the demands of the high-frequency action for vibrotactile feedback. During the cyclic test of 1 million cycles at 20 Hz, a 10% change of resistance per cycle was observed. This corresponds to an average strain rate of 400%/s (10% × 2 × 20 Hz) experienced by the SPA-skin for a million cycles, with continuous current consumption at 1.25 mA throughout the 14 h of testing period.

Dynamic characterization. Our SPA-skin can modulate the actuation amplitude over 100 Hz of dynamic range of frequencies derived from human mechanoreception capabilities. The SPA-skin is actuated with an on–off pressure input that is regulated at set amplitudes between [illegible] 30 kPa. The dynamic response shows an increase in relative change in resistance, $\Delta R/R_0$, concomitant to the increase of the actuation pressure at 5 Hz (Fig. 2d). The inflation and deflation behaviors of the sensor–actuator system are repeatable over a range of actuation frequencies, as seen in the five consecutive cycles shown in Figure 2c. The system dynamics resulting from the material elastic properties and the actuator geometry with φ 2 mm and tube length of 300 mm limit the maximum rate of change in inflation/deflation. This manifests as an increase in the baseline and a decrease in the maximum output as the operational frequency increases (Fig. 2e). The cutoff frequency of our SPA-skin design is measured to be 30 Hz, above which the actuation amplitude is less than 70% of its maximum value. Although the vibration amplitude decreases above 30 Hz, it is still measurable and perceivable to the human skin for the frequencies up to 100 Hz (Fig. 2f).[35] The measurement system can measure the resistance of sensor dynamically with accuracy of 0.4% at 1600 samples per second, which enabled recording of 16 samples at 100 Hz. This level of accuracy allowed for measurement of 25 distinct levels for 10% change in the measured strain of the SPA at 100 Hz.

Analytical model and control strategies

The static and dynamic characteristics of the SPA-skin show that the integrated system is repeatable and stable over a range of actuation frequencies and amplitudes. Therefore, the sensor feedback can be used to actively control the SPA inflation height if the relationship between actuation amplitude and measured resistance can be developed. When the mapping from inflation height to actuator strain is established, the output blocked force is zero in the absence of external loading. The blocked force is generated when an external loading blocks the actuator inflation. It is also important to note that the soft actuators exhibit complex mechanical behavior upon inflation due to the hyperelastic nature of the silicone materials. Such a behavior makes it complicated to accurately maintain the actuator inflation amplitude or output blocked force only with open-loop analytical model without a feedback sensing mechanism. We utilized the integrated resistive strain sensors to predict the average strain experienced by actuator and map it to the actuation height. We developed and experimentally verified an analytical model for the actuator behavior upon inflation, based on the results obtained from the integrated resistive sensor-skin, an external inflation height sensor, and an external pressure sensor (Fig. 3a). Our model maps the measured resistance change ($\Delta R/R_0$) from sensor to inflation height (h) analytically, based on the actuator inflation geometry and biaxial deformation of material upon inflation. In the first stage, we developed geometrical mapping function for the measured strain for a given inflation height (Fig. 3a). As the strain experienced by the sensor meanders is equibiaxial, we then map it to corresponding change in resistance value resulting from the actuator inflation.

Assuming a Poisson's ratio (v) of 0.5 for PDMS and an isotropic nature of the soft material, we can assume equibiaxial stress in the actuator membrane upon inflation. Also, the effect of reduction in the remaining dimensions ($-\varepsilon'$) for applied strain (ε) in one dimension for a given Poisson's ratio is:

$$(1-\varepsilon') = (1+\varepsilon)^{-v}. \tag{1}$$

Therefore, the change in dimensions of a single meander channel with length (l_0), width (w_0), and thickness (t_0) from equibiaxial strain upon inflation ($\varepsilon = \varepsilon_l = \varepsilon_w$) can be given as:

$$\begin{aligned} l &= l_0 + \Delta l_l - \Delta l_w = l_0\,(1+\varepsilon_l - \varepsilon'_w) = l_0[(1+\varepsilon)^{-v} + \varepsilon], \\ w &= w_0 - \Delta w_l + \Delta w_w = w_0(1-\varepsilon'_l + \varepsilon_w) = w_0\,[(1+\varepsilon)^{-v} + \varepsilon], \\ t &= t_0 - \Delta t_l - \Delta t_w = t_0\,(1-\varepsilon'_l + 1 - \varepsilon'_w - 1) = t_0[2(1+\varepsilon)^{-v} - 1], \end{aligned} \tag{2}$$

where $\Delta l_{l/w}$, $\Delta w_{l/w}$, and $\Delta t_{l/w}$ are changes in length, width, and height of the soft material due to strain in the direction of length/width (l/w), respectively.

Hence, the change in resistance of the biphasic metal encapsulated within the silicone membranes can be given as:

$$\frac{R}{R_0} = \frac{l/l_0}{(w/w_0)(t/t_0)} = \frac{1}{2(1+\varepsilon)^{-v} - 1}. \tag{3}$$

Furthermore, the correlation between uniaxial strain and actuator inflation height can be formulated using the volumetric change in the actuator and spatial distribution of sensor meanders on the actuator. The actuator of diameter (d) inflated to height (h) takes the approximate shape of a scooped sphere with a variable radius (r) (Fig. 3a, b). The radius decreases from infinity to 5 mm as actuator inflates from 0 to 5 mm height. The average uniaxial strain in a single meander during inflation to height can be described as:

$$\varepsilon = \frac{l - l_0}{l_0} = \frac{\sin^{-1}\frac{x}{r}}{\frac{x}{r}} - 1, \tag{4}$$

where x is the actuator radius, l is the final length, l_0 is initial length, and $r = \sqrt{x^2 + (r-h)^2}$. The sensor meander pattern

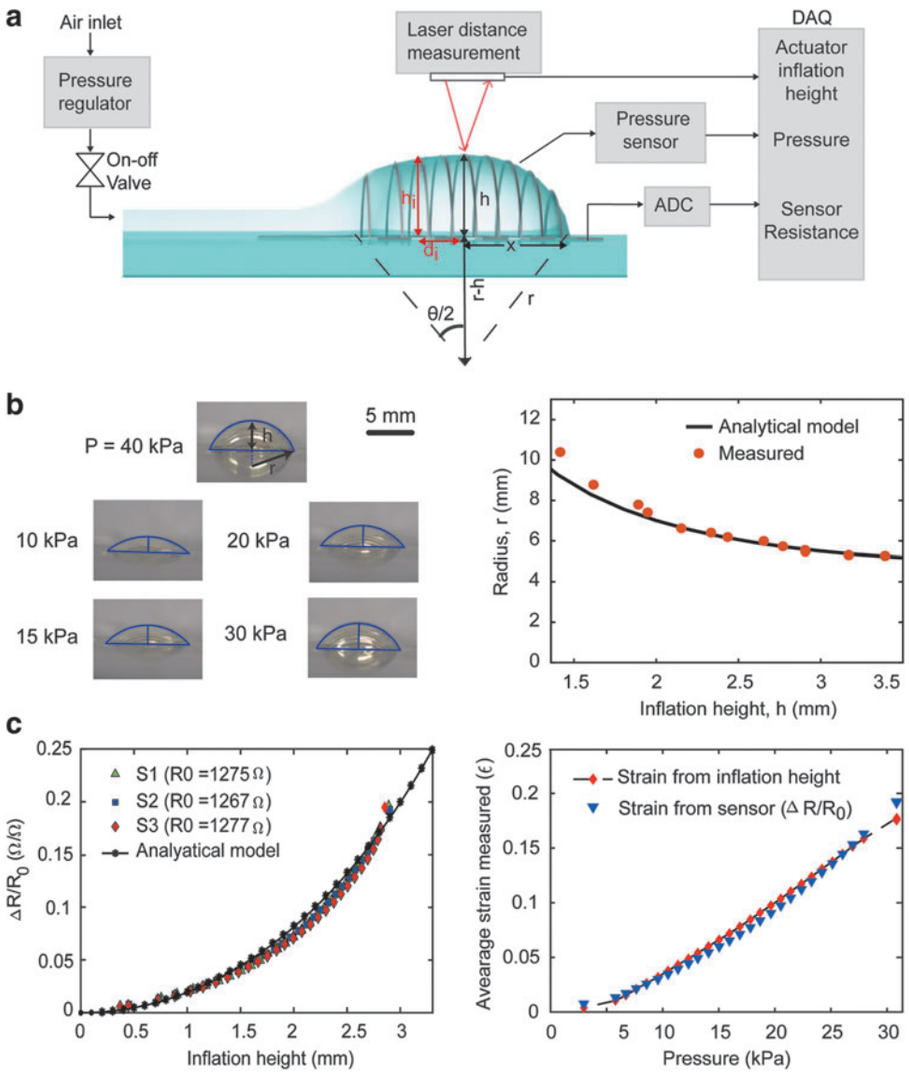


FIG. 3. Experimental setup and model. **(a)** Experimental setup for validating the sensor-embedded SPA-skin model upon actuation, overlaying the geometric parameters used in the analytical model. **(b)** Images showing the SPA inflation over a range of actuation pressures used to measure the inflation radius (r) and the inflation height (h) for geometrical model validation. The measured inflation radius is compared with the geometric model assuming the SPA inflation geometry as a part of a scooped sphere. **(c)** Average measured and computed strains for given inflation heights. **(d)** Average strain as a function of input pressure (*red dots*: model, *blue dots*: experimental strain measured by the resistive sensor). ◀4C

consists of 18 parallel lines equally distribute along the surface of the actuator membrane. The i^{th} stripe of the sensor channel is distance (d_i) from center of the actuator and during inflation reaches height (h_i):

$$h_i = h_{max} - r + \sqrt{r^2 - d_i^2}. \tag{5}$$

From Equations (3) and (4), the average strain experienced by all the sensor meanders on the actuator surface is given as:

$$\varepsilon_{\text{avg}} = \sum_{i=1}^{n} \frac{\varepsilon_i}{n} = \frac{1}{n} \sum_{i=1}^{n} \left\{ \frac{\sin^{-1} \frac{x}{r_i}}{\frac{x}{r_i}} - 1 \right\} \approx \frac{\Delta R}{R}, \tag{6}$$

where the GF is 1.[30]

Hence, to deduce the inflation height (h) by measuring change in resistance ($\Delta R/R_0$), an explicit mapping from $\Delta R/R_0 \rightarrow h$ is necessary. However, it is impossible to obtain, as Equation (2) is a coupled equation. Therefore, a piecewise polynomial curve fit is obtained for the inverse mapping of Equation (2) (Fig. 3c):

$$h = 49800\left(\frac{\Delta R}{R_0}\right)^3 - 2890\left(\frac{\Delta R}{R_0}\right)^2 + 74.6\left(\frac{\Delta R}{R_0}\right) + 0.109 \quad for\ 0 < \left(\frac{\Delta R}{R_0}\right) < 0.025$$

$$h = 33\left(\frac{\Delta R}{R_0}\right)^3 - 31\left(\frac{\Delta R}{R_0}\right)^2 + 16\left(\frac{\Delta R}{R_0}\right) + 0.63\ for\ 0.025 < \left(\frac{\Delta R}{R_0}\right) < 0.4,$$

with Error Norm = 0.0079.

Results

Experimental setup

High-speed actuation of the SPA-skin demands a test setup that provides a high data rate resistance measurement and a low settling time pressure regulation. We required at least

SORO-2019-0013-ver9-Sonar_1P.3d 08/19/19 9:02pm Page 6

1000 samples per second of sensor resistance values to ensure reliable and accurate estimation of actuator state, as a digital control system needs at least 8–10 times more samples than the actual operational frequency of the system (100 Hz for SPA-skin). We developed a custom 16-bit high-speed data acquisition system with a low on-resistance multiplexer, A/DC (ADS8517; TI) and an Arduino microcontroller board that measured the sensor resistance at 1600 Hz per channel with 0.4% accuracy (Fig. 3a). The low resistance multiplexer reduced the effect of extra resistance added in the sensor resistance measurement. It was also necessary to have a pressure regulator that can react within 10 ms to be able to control the SPA-skin at 100 Hz of vibratory output. In practice, we obtained settling time of 20 ms with a piezo-actuator drive pressure for maximum pressure change from 0 to 100 kPa that allowed us to control the SPA-skin up to 50 Hz. The Arduino microcontroller also directed the control commands to this piezo-pressure regulator to achieve the desired set point. The test setup is also equipped with an integrated pressure sensor (001BGAA5; Honeywell) and a laser interferometer (HG-C1030; Panasonic) to measure the SPA pressure and the inflation height, respectively. There is a micrometer placed vertically and connected to a high precision 3D force sensor (Nano 17; ATI Industrial Automation) for applying a controlled blocked force externally to simulate disturbances (Supplementary Fig. S3c).

Model validation

Our test setup enabled measurement of inflation height, input pressure, and strain sensor resistance to process the data for validation of the analytical model developed in the previous section. We measured the maximum height (h_{max}) during inflation at the given pressure with an external laser displacement sensor and recording the sensor response as depicted in Figure 3b. We inflated the SPA-skin at various input pressure and took images for fitting a curve of radius ''r'' and while simultaneously measuring the observed inflation height (h). The experimental values of curved fitted radii with the scooped sphere approximation for given inflation height matches closely with the expected geometrical model (Fig. 3b). Afterward, we derived the average strain values from Equation (5) and the external height sensor reading. Assuming the GF of 1, we obtained the analytical model plot of expected resistance change ($\frac{\Delta R}{R}$) for given inflation height in Figure 3c. The subsequent experimental measurements show that the resistance change over inflation height of the SPA-skin for three different samples is well in agreement with the analytical model (Fig. 3c and Supplementary Figure S2). This confirmed that the integrated strain sensor could effectively be used to measure the actuator inflation height, eliminating the dependency of actuator performance on the manufacturing variations and input pressure. Next, we developed a strain controller to have the strain sensor for active closed-loop control.

◀SF2

Active control of the force exerted by the SPA-skin

A coherent and responsive haptic feedback from deformable soft interfaces relies on explicit control of the actuation force and frequency, regardless of the loading conditions. If not, the wearer will feel unstable feedback depending on how the device is positioned. Hence, we demonstrated the closed-loop capabilities to actively adapt for the changes in the loading and provide a coherent tactile feedback. We designed a setup that uses a 1 cm^3 cube of Ecoflex 30 silicone[8] to simulate contact with the human skin, placed over the SPA-skin (Fig. 4a). Ecoflex 30 is selected as its compressive behavior is comparable with that of human skin.[38]

◀F4

We have the relationship between the measured resistance and the biaxial strain on the system from the analytical

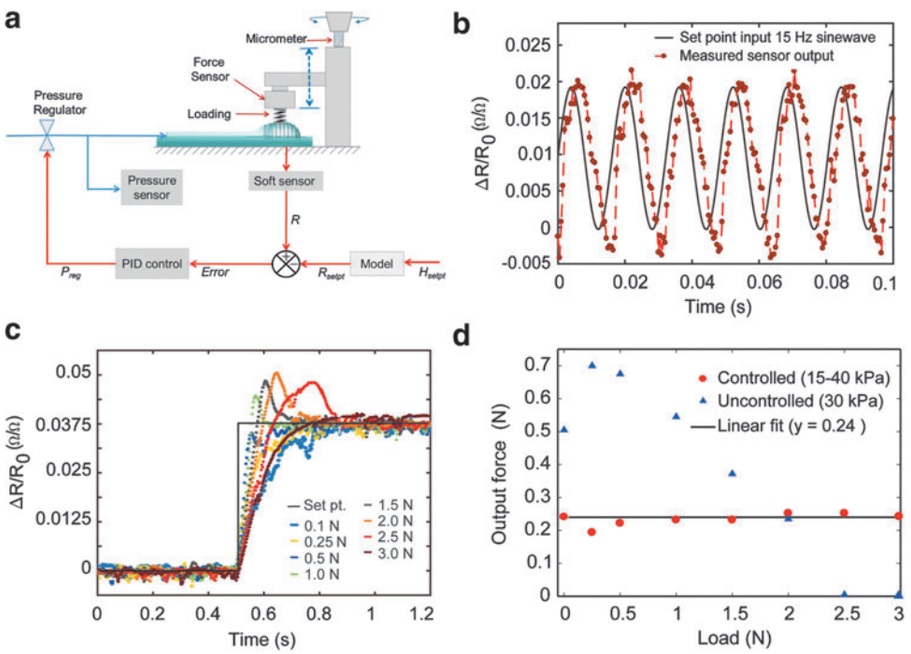


FIG. 4. Test bed for active closed-loop control. **(a)** Control flow diagram of the SPA-skin with a soft skin-like material placed between the actuator and an external force sensor, simulating external loading of the sensor against skin. A Vernier scale controls the displacement and therefore blocked force. **(b)** Controller tracking a sinusoidal perturbation of set point input at 15 Hz. **(c)** Controller performance under eight different loading conditions. The controller has a damped response at 3 N as the pressure required to achieve the set point exceeds the 40 kPa pressure controller safety limit. **(d)** Effect of loading on the SPA-skin performance when controlled using a pressure sensor and when using an integrated strain sensor to achieve a 0.25 N blocked force set point.

4C ▶

model. Under variable loading conditions, the actuator strain value maintained through closed-loop control will ensure uniform blocked force feedback to the wearer.

The inflation height or the expected strain value can be mapped to the desired resistance chance from the model developed previously. Hence, a PID controller is developed with this desired resistance change as a set point to control the input pressure for achieving constant inflation of the SPA-skin independent of the loading. An external pressure sensor is used as a safety mechanism to limit the SPA inflation to 40 kPa maximum (Fig. 4a). During the free unloaded operation, the control loop easily achieved the arbitrary strain set points (Fig. 4b and Supplementary Fig. S3). Additionally when external forces were introduced, the system continues to converge to the set point inflation, regardless of the preload (Fig. 4c). The feedback from the embedded strain sensors guarantees the desired actuation, even when the external loading is an order of magnitude higher than the desired blocked force produced by the SPA-skin (Fig. 4d). Eventually, as the loading increases, the system's mechanical inertia increases, which lead to an increase in the overshoot in the control (Fig. 4c). We tuned the PID gains conservatively to cover this fact and compensate for the overshoot, while degrading a little on the system settling time.

Conclusion

For an effective wearable technology, we require an accurate understanding of the physical interactions between the device and the wearer's perception. We engineered a closed-loop control of an entirely soft wearable haptic platform over a wide range of vibrotactile feedback.

The soft material-based design provided inherent safety much needed for a human–machine interaction as well as compliance matching with human skin to provide natural wearability. We prototyped a soft monolithic sensor-integrated SPA with embedded sensing and actuation capabilities and with soft sensors that have no mechanical loading impact on the actuator. The use of SPAs provided high bandwidth, simple design for iteration, and a highly customizable thin form factor as opposed to the traditionally available rigid vibration motors. The SPA-skin prototype produced forces up to 1 N with controllability of 0.05 N, and actuation dynamics of up to 100 Hz with controllability of 0.1 Hz; these are essential for providing a wide range of proprioceptive feedback to the wearer. The system characterization of the SPA-skin under continuous actuation and sensing showed robust and repeatable behavior over 1 million cycles, thereby promising compatibility with ''real-life'' wearable applications. We further demonstrated closed-loop control capabilities of this SPA-skin system at 15 Hz sinusoidal vibration at 1 kHz control speed. The closed-loop controller, based on an analytical model of the system, uses the sensor resistance to control the average strain of the actuator and allow for generating uniform output force under different loading conditions. This allowed the wearer to feel a consistent feedback independent of the wearing conditions. Furthermore, the bidirectional operations of the SPA-skin platform offer a wearable system that can not only be used for haptic feedback but also for quantification of human proprioceptive capabilities over range of frequencies. Specifically, the use of the SPA-skin in user studies will provide quantitative measurement of tactile feedback through integrated soft sensing to match with user's qualitative responses. The SPA-skin can be deployed as a distributed $n \times n$ array of sensor–actuator network for more complex tactile communication tasks. All these features make the SPA-skin a promising solution for applications demanding more intuitive and comprehensive tactile interactions.

Acknowledgments

The authors would like to thank the Swiss National Centre of Competence in Research (NCCR) Robotics, the European Research Project Proof of Concept grant (SoWe), and the Bertarelli Foundation.

Author Disclosure Statement

No competing financial interests exist.

Funding Information

Supplementary Material

Supplementary Figure S1
Supplementary Figure S2
Supplementary Figure S3
Supplementary Movie S1

References

1. Minogue J, Jones MG. Haptics in education: exploring an untapped sensory modality. Rev Educ Res 2006;76:317–348.
2. Sigrist R, Rauter G, Riener R, *et al.* Augmented visual, auditory, haptic, and multimodal feedback in motor learning: a review. Psychon Bull Rev 2013;20:21–53.
3. Westebring-van der Putten EP, Goossens RHM, Jakimowicz JJ, *et al.* Haptics in minimally invasive surgery—a review. Minim Invasive Ther Allied Technol 2008;17:3–16.
4. Alahakone AU, Senanayake SMNA. Vibrotactile feedback systems: current trends in rehabilitation, sports and information display. In 2009 IEEE/ASME International Conference on Advanced Intelligent Mechatronics. 2009, pp. 1148–1153.
5. Hayward V, Astley OR, Cruz-Hernandez M, et al. Haptic interfaces and devices. Sens Rev 2004;24:16–29.
6. Vibration Motors. Precision Microdrives. Available at: https://www.precisionmicrodrives.com/vibration-motors.
7. Johnston ID, McCluskey DK, Tan CKL, *et al.* Mechanical characterization of bulk Sylgard 184 for microfluidics and microengineering. J Micromech Microeng 2014;24:035017.
8. Ecoflex® 00–30 Product Information. Smooth-On, Inc. [Online]. Available at: https://www.smooth-on.com/products/ecoflex-00-30/.
9. Diridollou S, Patat F, Gens F, et al. In vivo model of the mechanical properties of the human skin under suction. Skin Res Technol 6:214–221.
10. Case JC, White EL, Kramer RK. Soft material characterization for robotic applications. Soft Robot 2015;2:80–87.
11. Alici G. Softer is harder: what differentiates soft robotics from hard robotics?. MRS Adv 2018;3:1557–1568.
12. Choi S, Kuchenbecker KJ. Vibrotactile display: perception, technology, and applications. Proc IEEE 2013;101:2093–2104.

SORO-2019-0013-ver9-Sonar_1P.3d 08/19/19 9:02pm Page 8

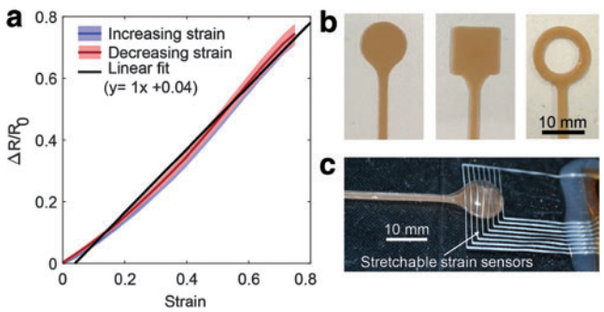
13. Bauer S, Bauer-Gogonea S, Graz I, *et al.* 25th anniversary article: a soft future: from robots and sensor skin to energy harvesters. Adv Mater 2014;26:149–162.
14. Yun S, Kang BB, Cho K. Exo-glove PM: an easily customizable modularized pneumatic assistive glove. IEEE Robot Autom Lett 2017;2:1725–1732.
15. Hawkes EW, Blumenschein LH, Greer JD, *et al.* A soft robot that navigates its environment through growth. Sci Robot 2017;2:eaan3028.
16. Polygerinos P, Correll Nikolaus, Morin SA, *et al.* Soft robotics: review of fluid-driven intrinsically soft devices; manufacturing, sensing, control, and applications in human-robot interaction. Adv Eng Mater 2017;19:1700016.
17. Cianchetti M, Laschi C, Menciassi A, *et al.* Biomedical applications of soft robotics. Nat Rev Mater 2018;3:143.
AU12 18. Agharese N, Cloyd T, Blumenschein LH, *et al.* HapWRAP: soft growing wearable haptic device. In 2018 IEEE International Conference on Robotics and Automation (ICRA), 2018, pp. 1–5.
19. Phung H, Nguyen CT, Nguyen TD, *et al.* Tactile display with rigid coupling based on soft actuator. Meccanica 2015; 50:2825–2837.
20. Marette A, Poulin A, Besse N, *et al.* Flexible zinc–tin oxide thin film transistors operating at 1 kV for integrated switching of dielectric elastomer actuators arrays. Adv Mater 2017;29:1700880.
21. Moseley P, Florez JM, Sonar HA, *et al.* Modeling, design, and development of soft pneumatic actuators with finite element method. Adv Eng Mater 2016;18:978–988.
22. Agarwal G, Besuchet N, Audergon B, *et al.* Stretchable materials for robust soft actuators towards assistive wearable devices. Sci Rep 2016;6:34224.
23. Martinez RV, Glavan AC, Keplinger C, *et al.* Soft actuators and robots that are resistant to mechanical damage. Adv Funct Mater 2014;24:3003–3010.
24. Mosadegh B, Polygerinos P, Keplinger C, *et al.* Pneumatic networks for soft robotics that actuate rapidly. Adv Funct Mater 2014;24:2163–2170.
25. Robertson MA, Paik J. New soft robots really suck: vacuum-powered systems empower diverse capabilities. Sci Robot 2017;2:eaan6357.
26. Larson C, Peele B, Li S, *et al.* Highly stretchable electroluminescent skin for optical signaling and tactile sensing. Science 2016;351:1071–1074.
AU13 27. Shintake J, Sonar H, Piskarev E, *et al.* Soft pneumatic gelatin actuator for edible robotics. In 2017 IEEE/RSJ International Conference on Intelligent Robots and Systems (IROS). 2017, pp. 6221–6226.
28. Rus D, Tolley MT. Design, fabrication and control of soft robots. Nature 2015;521:467–475.
29. Trung TQ, Lee N. Flexible and Stretchable Physical Sensor Integrated Platforms for Wearable Human-Activity Monitoringand Personal Healthcare. Adv Mater 2016;28:4338–4372.
30. Hirsch A, Michaud HO, Gerratt AP, *et al.* Intrinsically stretchable biphasic (solid–liquid) thin metal films. Adv Mater 2016;28:4507–4512.
31. Nam S, Yun S, Yoon JW, *et al.* A robust soft lens for tunable camera application using dielectric elastomer actuators. Soft Robot 2018. [Epub ahead of print]; DOI: 10.1089/soro.2017.0146.
32. Mößinger H, Haus H, Kauer M, *et al.* Tactile feedback to the palm using arbitrarily shaped DEA. Presented at the Electroactive Polymer Actuators and Devices (EAPAD) 2014. 2014;9056:90563C.
33. Truby RL, Wehner MF, Grosskopf AK, *et al.* Soft somatosensitive actuators via embedded 3D printing. Adv Mater 2018;30:1706383.
34. Sonar HA, Paik J. Soft pneumatic actuator skin with piezoelectric sensors for vibrotactile feedback. Front Robot AI. 2016;2.
35. Mortimer BJP, Zets GA, Cholewiak RW. Vibrotactile transduction and transducers. J Acoust Soc Am 2007;121: 2970–2977.
36. Kaczmarek KA, Webster JG, Bach-y-Rita P, *et al.* Electrotactile and vibrotactile displays for sensory substitution systems. IEEE Trans Biomed Eng 1991;38:1–16.
37. Schneider F, Wallrabe U, Fellner T, *et al.* Mechanical properties of silicones for MEMS. J Micromech Microeng 2008;18:065008.
38. Sparks JL, Vavalle NA, Kasting KE, *et al.* Use of silicone materials to simulate tissue biomechanics as related to deep tissue injury. Adv Skin Wound Care 2015;28:59–68.

Address correspondence to: ◀AU14
Jamie Paik
Reconfigurable Robotics Laboratory
Ecole Polytechnique Fédérale de Lausanne
Lausanne 1015
Switzerland

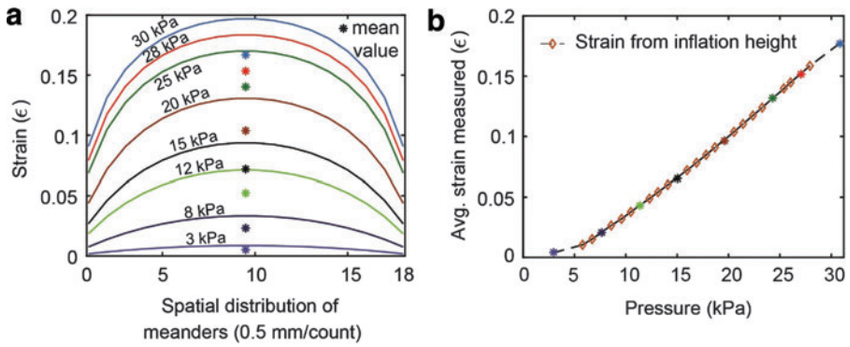
E-mail: jamie.paik@epfl.ch

Supplementary Data

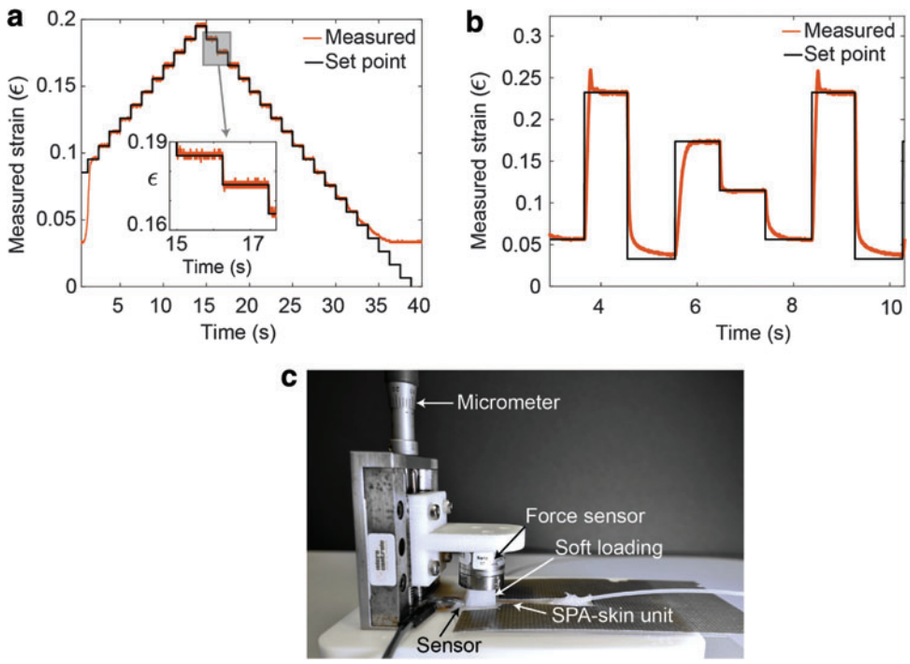
SUPPLEMENTARY MOVIE S1. SPA-skin operation at low frequency (5 Hz) and high frequency (50 Hz). SPA, soft pneumatic actuator.



SUPPLEMENTARY FIG. S1. Stretchable strain sensor characterization and sample sensor, actuator designs. **(a)** Average nominal sensor resistance change with standard deviation for strain rates: 0.018, 0.18, and 1.8 mm/s in increasing and decreasing directions of the applied uniaxial strain. The linear fit for the average resistance change gives GF of ''1.'' **(b)** Three sample designs of SPA, demonstrating the configurability and distributability of the SPA-skin design. The *brown-colored mask* determines the inflation region for SPA. **(c)** An SPA-skin prototype design flexibility of the sensor–actuator system, with eight independent sensors 100 μm apart placed on a 10 mm diameter actuator. GF, gauge factor; SPA, soft pneumatic actuator.



SUPPLEMENTARY FIG. S2. Experimental validation of the analytical model. **(a)** The analytical model predicting uniaxial strain over each sensor meander using the measured inflation height. The mean value of the sensor strain determines the measured change in the resistance of the sensor. **(b)** The measured average strain from the analytical model is plotted with respect to the actuator input pressure. Each *colored (*) marker* maps to the corresponding mean value of the strain in Supplementary Figure S2c and is then used to validate the strain model with measurements from sensor resistance (Fig. 3c). ◀AU15



SUPPLEMENTARY FIG. S3. Closed-loop controller evaluation and test bed design. **(a)** A staircase set point tracking using integrated stretchable strain sensor and external pressure regulation shows high precision performance of the controller to control the SPA-skin system. The controller cannot track the actuator state below 3% strain set point, as the SPA cannot be deflated further without an external preloading. **(b)** In the second test case, an arbitrary set point tracking test shows the stability of PID-controller over the full range of safe actuation (0–25% strain at 35 kPa) for the SPA-skin unit. **(c)** The physical test bed used to validate the SPA-skin system model and test the active closed-loop controller performance. This test bed consists of a precision micrometer to control the preload, a force sensor, a soft silicone preload to simulate the human skin, a pressure regulator, a microcontroller, and a sensor readout electronics. PID. ◀AU16

AUTHOR QUERY FOR SORO-2019-0013-VER9-SONAR_1P

AU1: Please identify (highlight or circle) all authors' surnames for accurate indexing citations.
AU2: Please check the correctness of authors' affiliations.
AU3: The Publisher requests for readability that no paragraph exceeds 15 typeset lines. Please check for long paragraphs and divide where needed.
AU4: Supplementary Fig S1 is not cited in the main doc. Please insert the citation in the main doc.
AU5: Please define ''PID.''
AU6: Author Disclosure accurate? If not, please amend as needed.
AU7: Please provide funding information. Include the full name (no abbreviations) of funding agency(ies)/institution(s) and grant numbers. Ensure the accuracy of this information. If no funding was received, please clearly state as such.
AU8: References 19 and 20 are not cited in the text. Please insert the citation in the text.
AU9: In Ref. 4, please mention the location.
AU10: Please provide the date you last viewed the website for Reference 6.
AU11: Please provide the date you last viewed the website for Reference 8.
AU12: In Ref. 18, please mention the location.
AU13: In Ref. 27, please mention the location.
AU14: Please confirm the address of correspondence.
AU15: Please check the usage of the citation ''Supplementary Figure S2c'' in Supplementary Figure S2 legend since label ''c'' is not provided for Supplementary Figure S2.
AU16: Please define ''PID.''